Hydrodynamic model of directional ciliary-beat organization in human airways

SIMON GSELL[1⋆], ETIENNE LOISEAU[2], UMBERTO D'ORTONA[1], ANNIE VIALLAT[2], JULIEN FAVIER[1]
[1]Aix Marseille Univ, CNRS, Centrale Marseille, M2P2, Marseille, France
[2]Aix Marseille Univ, CNRS, CINAM, Marseille, France
⋆simon.gsell@univ-amu.fr

Abstract

In the lung, the airway surface is protected by mucus, whose transport and evacuation is ensured through active ciliary beating. The mechanisms governing the long-range directional organization of ciliary beats, required for effective mucus transport, are much debated. Here, we experimentally show on human bronchial epithelium reconstituted *in-vitro* that the dynamics of ciliary-beat orientation is closely connected to hydrodynamic effects. To examine the fundamental mechanisms of this self-organization process, we build a two-dimensional model in which the hydrodynamic coupling between cilia is provided by a streamwise-alignment rule governing the local orientation of the ciliary forcing. A phase transition from local mucus recirculations to a long-range unidirectional mucus flow allowing effective clearance is predicted at high ciliary density and a high mucus viscosity, as experimentally observed. In the latter case, we show that in a tube geometry mimicking a virtual bronchus, the transport direction spontaneously aligns with the distal-proximal axis.

1 Introduction

Billions of microscopic active cilia on the surface of the bronchial epithelium propel a viscous fluid, called mucus. Its function is to capture and eliminate inhaled pathogens, allergens and pollutants (Wanner et al., 1996). This process, referred to as mucociliary clearance, is impaired in respiratory diseases such as primary dyskinesia, severe asthma (Chanez, 2005), COPD (Hogg et al., 2004) and cystic fibrosis (Regnis et al., 1994, Boucher, 2007), which affect hundreds of millions of people worldwide.

The transport of mucus requires a long-range coordination of ciliary beat directions along the airways. In *in-vitro* cell cultures, observations of large-scale circular mucus flows spanning the culture chamber was reported by Matsui et al. (1998). Recently, Khelloufi et al. (2018) showed that this swirly transport is associated with a circular order of the ciliary beating directions underneath the mucus. Furthermore, mucus swirls of various sizes were observed, whose size was shown to scale with the ciliary density. Due to the invasive nature of *in-vivo* experiments, the mechanisms underlying mucus transport and collective dynamics of the ciliary activity remain poorly understood. In particular, the mechanisms involved in the directional self-organization of the ciliary beats over distances spanning the bronchi and trachea are yet to be elucidated. At the tissue scale, the planar polarization of the epithelial ciliated cells, established during development, is expected to determine the rotational polarity of the basal body at the base of the cilia, which sets the direction of beating (Wallingford, 2010, Spassky and Meunier, 2017). However, daily variations of ciliary-driven cerebrospinal fluid flow patterns have recently been observed in *in-vivo* mouse brain ventricles (Faubel et al., 2016). In addition, Guirao et al. (2010) showed that ciliary-beat directions on cell cultures issued from the subventrical zone of newborn mice could be drastically changed by applying an external flow. Finally, the directional collective order of ciliary beats on the multiciliated skin cells of the *Xenopus* embryo could be refined by applying an external flow to skin

explants (Mitchell et al., 2007). These phenomena strongly suggest the existence of a coupling between hydrodynamics and long-range ciliary-beat orientation for at least two animal models. However, despite these experimental evidences, no physical model has been proposed so far to investigate the emergence of orientational order driven by hydrodynamic effects on a ciliated epithelium. In the context of mucociliary clearance, such model could be highly beneficial for the comprehension, prediction and control of this crucial physiological process.

Physical models of collective behavior have already been developed to describe the patterns of motion emerging in groups of interacting active individuals, such as insect swarms, bird flocks, fish schools or bacterial colonies (Vicsek and Zafeiris, 2012, Sumpter, 2010, Saintillan, 2018). These models, deriving from the seminal work of Vicsek et al. (1995), are based on interaction rules between moving individuals, namely avoidance, attraction and alignment. The role of each interaction on the resulting pattern, such as polarized schools and mills has been finely analyzed by Costanzo and Hemelrijk (2018). Yet, the long-range organization of ciliated epithelia cannot be described by these models since ciliated cells are non-motile. New models are thus needed to tackle collective effects involved in this specific active system composed of hydrodynamically-coupled static elements.

Here, we experimentally show on human bronchial epithelia reconstituted *in-vitro* that, in presence of a ciliary-driven mucus flow on the epithelial surface, directions of ciliary beats tend to align progressively along mucus streamlines. Conversely, upon mucus removal, the orientational order of ciliary beat is lost. Based on these observations, we propose a two-dimensional hydrodynamic model of ciliary-beat organization where the ciliary orientation is controlled by a streamwise-alignment rule. In this model, the coupling between distant cilia is ensured only by the hydrodynamics. The model relies on two independent physical quantities, namely (i) the ciliary density and (ii) the viscosity ratio between mucus and the periciliary layer. We establish a phase diagram of mucus flow patterns, which predicts a transition between local mucus recirculations obtained for low ciliary densities and viscosity ratios, and a long-range unidirectional flow associated with an effective mucus clearance for high ciliary densities and viscosity ratios. Finally, in this latter case, we show that in a virtual bronchus the direction of transport aligns with the distal-proximal axis.

Results

Ciliary beat reorientation in human bronchial epithelium cultures

The experimental system consists of well-differentiated human airway cultures at the air-liquid interface (ALI). These cultures exhibit the pseudo-stratified structure typical of bronchial epithelium, with basal cells, goblet cells that produce mucus, and ciliated cells with beating cilia (Khelloufi et al., 2018). The ciliary density on mature epithelium reaches around 70% of the epithelial surface. At high ciliary densities, the mucus is transported over macroscopic distances (see movie 1) thanks to the continuous beating of cilia. We image both the flow of mucus and the beating cilia underneath (movies 1 & 2). We then quantify the mucus flow direction as well as the beating directions of cilia (Fig. 1 and movie 2). Locally the cilia does not necessarily beat along the mucus flow direction (Fig. 1(a)) but they present an average direction at large scale. Yet, we show that the ciliary beating directions tend to align along the direction of mucus flow (Figs. 1(a,b) and movies 1 & 2) in a slow process of a maximum 35-40 angle reorientation

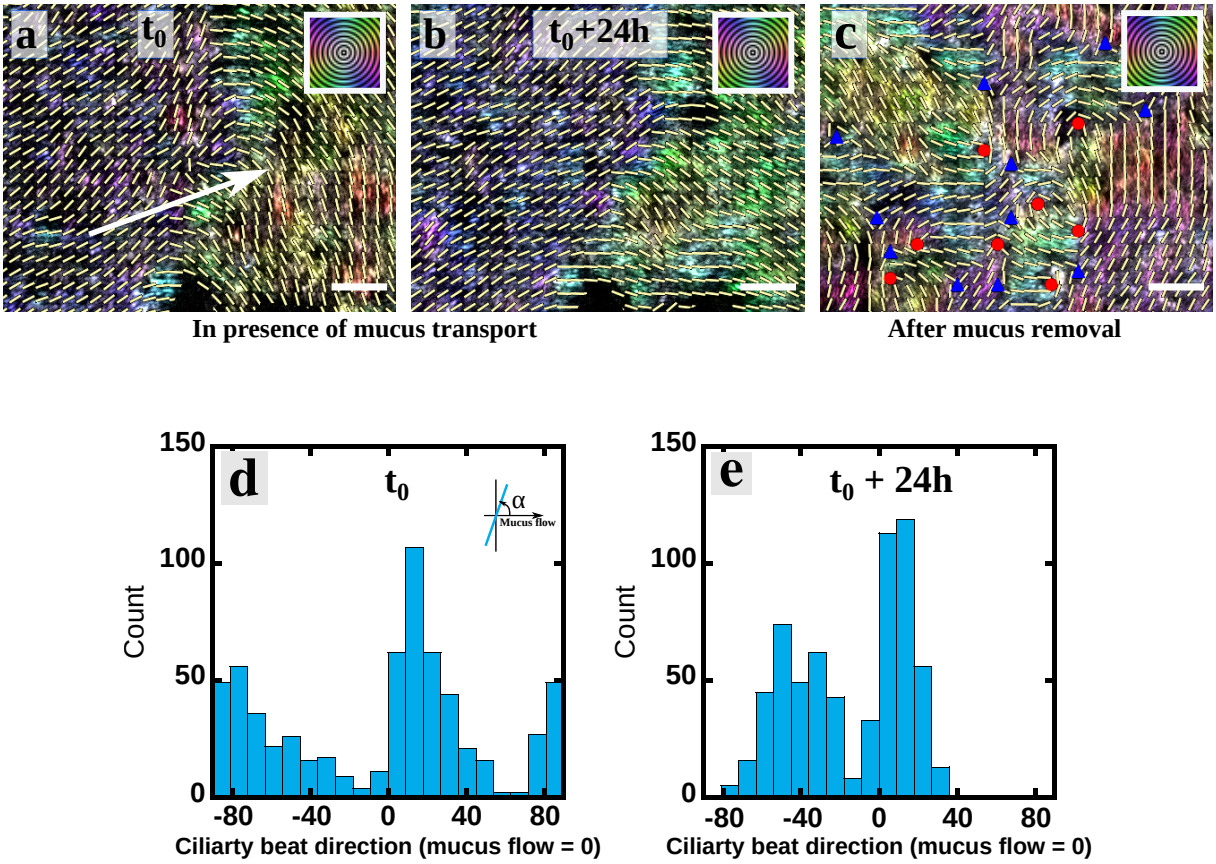

Figure 1: **Mucus transport reorients the beating direction of cilia** (a-b) Orientation maps of beating cilia at 24h interval while some mucus is transported above. The colors code for the direction of beating according to the orientation scale on the top right hand corner. The director field of the beating direction is plotted as an overlay and is averaged in boxes of 5 m x 5 m (∼ size of a ciliated cell). The white arrow indicates the averaged direction of the mucus transport in the considered field and is determined from movie 1. Within 24 hours some reorientations occur, in particular on the right-hand side of the image, and the beating direction can rotate up to 30-35 . (c) Orientation map of beating cilia 3 days after washing out the mucus with culture medium. The field of view is the same than in a & b. Colored triangles and circles indicate discontinuities in the director field. Scale bars are 20 m. The three field of views are representative of the whole culture chamber. The movie of the beating cilia corresponding to the three panels is movie 2. (d,e) Angle distributions of ciliary beats corresponding to the figures (a) & (b) respectively. The 0 orientation corresponds to the mucus flow direction. In presence of a transported mucus above the cilia, we observe a dynamic reorientation of the ciliary beat directions. Over 24h the two peaks of the distribution get more narrow and there is a shift of the two peaks toward the direction of the mucus flow measured from movie 1.

within 24 hours (see angle distributions in Figs. 1(d,e)). In contrast, when mucus is washed out from the surface of the cell culture and replaced with culture medium, we observe within three days a loss of the coordination of beating directions (Fig. 1(c)), highlighted by the emergence of numerous discontinuities in the director field of the beating cilia. At this stage, only small patches of cilia attached to neighboring

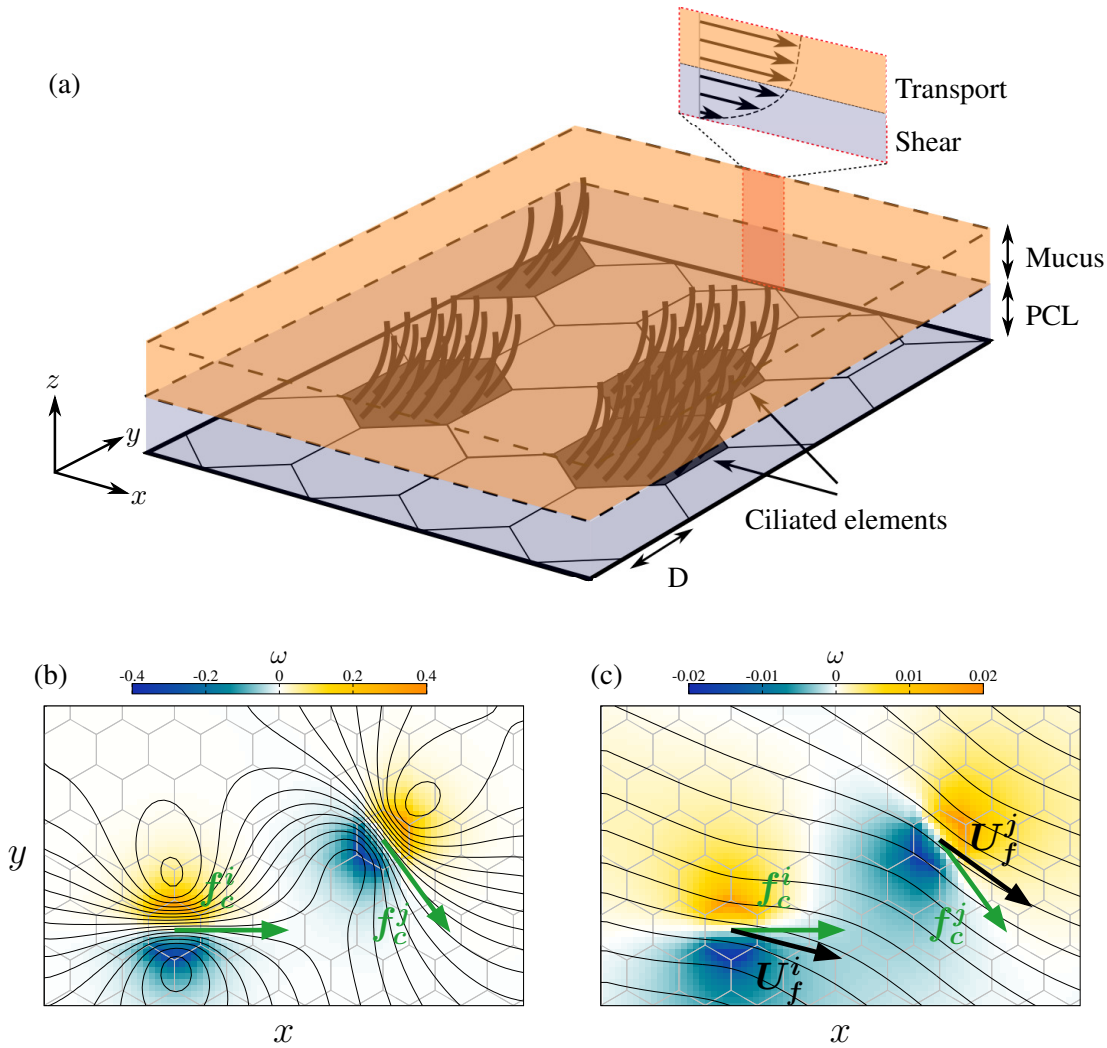

Figure 2: **Model of ciliary-driven mucus flow** – (a) Schematic view of the model of bronchial epithelium. (b,c) Typical flow in the vicinity of two ciliated elements i and j, for (b) $\lambda = 1$ and (c) $\lambda = 5$. The flow is visualized by streamlines and iso-contours of the flow vorticity. The hexagonal mesh is represented by gray lines. The ciliary forces ($\boldsymbol{f_c^i}$, $\boldsymbol{f_c^j}$) are indicated by green arrows. In (b), black arrows show the locally-averaged flow velocities($\boldsymbol{U_f^i}$, $\boldsymbol{U_f^j}$).

ciliated cells present the same beating direction. The characteristic diameter of these patches is around 10 to 20 m, corresponding to groups of 5 to 15 cells. These patches can be seen as unit elements of beating direction, likely constituted by ciliated cells having a common cell polarity. There is no transport of fluid at large scale anymore. These observations disclose the existence of a strong mucus-cilia interplay and that mucus flow triggers an active response of cilia driving their reorientation.

Hydrodynamic model of ciliary-beat organization

We assume that the hydrodynamic forces generated by the mucus flow drives the observed long range self-organization of the directions of ciliary beats, and propose the following two-dimensional model to examine this hypothesis. It is schematized in Fig. 2(a).

Locally, ciliary beats exert a force on the mucus. Considering a simple modelling of this force, the overall mucus flow resulting from the joint forcing of all ciliated cells is computed by solving the Navier-Stokes equations. The model is based on a streamwise-orientation hypothesis: ciliary beats, and the associated local forces, reorient in response to the computed mucus flow and gradually align with the local flow direction. Such system, initialized with random orientations of the ciliary beats, thus evolves towards a self-organized solution. Distant cilia interact with each other through their individual contribution to the overall forcing field driving the global mucus flow.

In practice, the plane epithelium surface is discretized using hexagonal unit elements, which represent cells or groups of cells (see Fig. 2(a)). Their side length is denoted by D. Two types of unit elements are considered, namely multi-ciliated cells, or groups of neighboring multi-ciliated cells that exhibit a joint ciliary-beat direction, and *passive* elements that represent club and goblet cells and, possibly, dysfunctional ciliated cells. We chose a random spatial distribution of these elements on the epithelium, in agreement with observations (Guirao et al., 2010).

The surface fluid consists of two layers, a low-viscosity periciliary layer (PCL), in which cilia beat, and a high-viscosity mucus layer (Wanner et al., 1996). The PCL thickness is about the cilia length. The PCL is a shear region; the fluid velocity, in the plane parallel to the epithelium, is zero on the epithelial surface and is equal to the mucus velocity at the PCL/mucus interface (Ding et al., 2014, Chateau et al., 2017)(see Fig. 2(a)). The mucus layer is modeled as a transport zone. Its velocity is parallel to the epithelial plane and is uniform along the z axis, as schematized in Fig. 2(a). Here the considered propelling force is spatially averaged over a group of cilia of one or more neighboring multi-ciliated cells (unit element), and temporally over a period longer than the cilium beat period.

Mucus is modeled as a Newtonian fluid, characterized by its density ρ_m and dynamic viscosity μ_m. The flow is governed by the two-dimensional incompressible Navier-Stokes equations. The flow momentum writes

$$\frac{\mathcal{D}(\rho_m \boldsymbol{U})}{\mathcal{D}t} = -\nabla P + \mu_m \nabla^2 \boldsymbol{U} + \boldsymbol{f_n}, \tag{1}$$

where $\mathcal{D}/\mathcal{D}t$ denotes the material derivative, and $\boldsymbol{U}$ and P are the flow velocity and pressure. The momentum flux occurring along the non-resolved direction, i.e. z axis, is modeled by a body force (i.e. momentum source or sink) $\boldsymbol{f_n}$ exerted on the mucus. Two types of momentum sources are considered. The first one results from the shear stress in the PCL; it linearly depends on the mucus velocity $\boldsymbol{U}$, namely $\boldsymbol{f_v} = -\kappa \boldsymbol{U}$, with κ a parameter called the PCL friction coefficient. The second force component, called the ciliary force and denoted by $\boldsymbol{f_c}$, results from the ciliary beating; it is non-zero on ciliated elements, and vanishes elsewhere. Its magnitude $|\boldsymbol{f_c}|$ is the same on all ciliated elements and is considered to be time independent, i.e. it represents the ciliary forcing averaged over one ciliary-beating period, as in Guirao and Joanny (2007). Overall, the total momentum source in Eq. 1 is expressed as $\boldsymbol{f_n} = \boldsymbol{f_v} + \boldsymbol{f_c}$.

The orientation of $\boldsymbol{f_c}$, defined by the angle θ_c^i on the i-th ciliated cell, is driven by a streamwise-alignment rule. The angle difference between the local flow and the beating direction is $\Delta\theta^i = \theta_c^i - \theta_f^i$, where θ_f^i

is the flow velocity averaged over the i-th ciliated element. The alignment rule follows

$$\theta_c^i(t+\Delta t) = \theta_c^i(t) + \Omega \frac{\Delta\theta^i(t)}{|\Delta\theta^i(t)|}\Delta t, \quad \Delta\theta^i(t) > \theta_0, \tag{2a}$$

$$\theta_c^i(t+\Delta t) = \theta_c^i(t), \qquad \Delta\theta^i(t) \leq \theta_0 \tag{2b}$$

where Δt is the model time step, Ω is a fixed angular velocity and θ_0 is an angle threshold. This alignment rule provides the hydrodynamic interaction mechanism between ciliated elements. More details on the implemented alignment rule are reported in *Material and Methods*.

Solutions of Eq. 1 are found using numerical simulations. Periodic conditions are set at the boundaries of the computational domain. The total number of ciliated elements in the domain is chosen according to the prescribed ciliary density $\phi = \frac{S_c}{S}$, where S_c designates the ciliated area and S is the total area. All computations are initialized with random orientations of the ciliated elements.

Overall, the model depends on six physical parameters, namely ρ_m, μ_m, ϕ, D, $|\boldsymbol{f_c}|$ and κ. The PCL friction coefficient κ is assumed to relate to PCL properties. From dimensional analysis, it writes $\kappa \sim \mu_p/\delta_p^2$, where μ_p and δ_p are the dynamic viscosity and thickness of the periciliary layer. In this model, mucus transport results from the competition between the ciliary forcing and the friction forcing. Accordingly, a typical mucus flow velocity can be derived from $|\boldsymbol{f_c}|$ and κ, namely $U_0 = |\boldsymbol{f_c}|/\kappa$. This indicates that the mucus velocity is assumed to mainly depend on the ciliary forcing and PCL properties. Following the Buckingham theorem, the number of parameters can be reduced to three non-dimensional and independent physical parameters, (i) the ciliary density ϕ, (ii) the Reynolds number $Re = \rho_m D U_0/\mu_m$ which represents the ratio between inertial and viscous forces and (iii) the non-dimensional interaction length λ, defined as

$$\lambda = \frac{\sqrt{\mu_m/\kappa}}{D}. \tag{3}$$

The λ parameter represents the typical range of influence of a ciliated element, resulting from the competition between viscous momentum diffusion over the epithelial plane and dissipation due to the friction force $\boldsymbol{f_v}$. Indeed, if λ is large (i.e. high mucus viscosity), the momentum transferred to the fluid through ciliary beating is rapidly diffused over a large fluid region; the limit case is the solid behavior, where the localized ciliary forcing is instantaneously transferred all over the material. In contrast, the range of influence decreases when λ is small, since the flow momentum tends to be damped faster than it is transported over the epithelial plane. Ciliated cells interact with each other only if their separation distance is low enough compared to their individual range of influence. Therefore, λ is referred to as hydrodynamic interaction length. Considering the above-mentioned connections between κ and the PCL properties, the interaction length is closely related to the mucus/PCL viscosity ratio, namely

$$\lambda \sim \frac{\delta_p}{D}\sqrt{\frac{\mu_m}{\mu_p}}. \tag{4}$$

The role of λ is illustrated in Figs. 2(b,c), which show the typical flow in the vicinity of two ciliated elements, denoted by i and j. The non-dimensional flow vorticity is defined as $\omega = \frac{D}{U_0}|\nabla \times \boldsymbol{U}|$. In the figure, high values of the vorticity (either positive or negative) emphasize fluid regions that are sheared along the epithelial plane, as an effect of the ciliary forcing. In this illustrative example, the ciliary force directions are fixed, i.e. the alignment rule Eq. 2 has been ignored. For low values of λ (Fig. 2(b)), shear

regions remain localized in the vicinity of the ciliated cells, and streamlines crossing the ciliated elements are mostly parallel to ciliary forces. Therefore, $\Delta\theta^i \approx \Delta\theta^j \approx 0$, and Eq. 2b is satisfied. For larger values of λ (Fig. 2(c)), large shear regions are observed, even though of lower magnitude than in the previous case, and flows induced by both ciliated cells tend to interact with each other. Consequently, streamlines are not parallel to ciliary forces, as illustrated by the locally-averaged flow velocities indicated in the figure. In this case, a trigger of the alignment rule Eq. 2 induces a re-alignment of the cells. This illustrates that λ is expected to control hydrodynamic interactions between ciliated elements.

Physiologically-relevant numerical values

To determine a relevant range of ϕ and λ for the simulations, one has to estimate their physiological range. During the ciliogenesis, the cilia density increases from 0 up to a final value of 70 % which corresponds to the cilia density in the bronchus (Raman et al., 2009, Staudt et al., 2014). The relevant values of λ can be estimated from Eq. 4. The size D for the unit elements is estimated from the size of the ciliated patches with the same beating direction, which, as seen in Fig. 1, is of the order of $D \approx 2 \times 10^{-5}$m. The thickness of the PCL has been measured by Button et al. (2012) and is of the order of $\delta_p \approx 10^{-5}$m. It is accepted that the PCL viscosity is close to that of water (Button et al., 2012) $\mu_p \sim 10^{-3} Pa.s$. The literature reports an important variability of mucus viscosity due to its heterogeneities, variations along the bronchial tree and clinical state of people. Values ranging from $\mu_m = 10^{-2} Pa.s$ to $\mu_m = 10^{2} Pa.s$ have been reported in prior works (Lai et al., 2009). The resulting range of a physiological λ, based on (4), is then in the range $[1.5, 150]$. Finally, it should be mentioned that the flow behavior is expected to be governed by viscous effects, i.e. $Re \ll 1$.

Three different mucus flow regimes: localized, swirly, long-range aligned

A square domain composed of approximately 10^4 elements is first considered. The Reynolds number is set to 0.1, and the flow solution is computed for λ and ϕ in the respective ranges of $\lambda \in [1, 150]$ and $\phi \in [0.1, 0.7]$. The system dynamics is computed until a steady state is reached, when the ciliary-beat organization and the related mucus flow remain constant in time (see movies 3, 4 and 5 for examples of transient dynamics). In this state, the ciliary forces and the flow are aligned locally. Three regimes associated with distinct flow patterns and ciliary-beat organizations are identified, as illustrated in Fig. 3.

When the ciliary density ϕ and the interaction length λ are small, typically $\phi = 0.1$ and $\lambda = 1$, a poorly organized regime is observed (Fig. 3(a)). Only local ciliary-beat alignments are observed in regions of high local ciliary densities. No large-scale flow pattern emerges. The flow length scale is of the order of the typical cell size, as indicated by the localized and short-range shear regions close to ciliated elements.

When ϕ and λ are larger, typically $\phi = 0.4$ and $\lambda = 2$ (Fig. 3(b)), a remarkable swirly pattern, associated with local mucus recirculations, emerges. The ciliary beat orientation exhibits circular alignments over length scales much larger than the typical cell size, emphasizing the emergence of large-scale collective behavior. These large vortices are associated with large-scale vorticity regions. Both clockwise and counter-clockwise flow circulations are observed, as shown by the negative (blue) and positive (yellow) values of the vorticity.

When ciliary density and interaction length are further increased (Fig. 3(c)), typically $\phi = 0.55$ and $\lambda =$

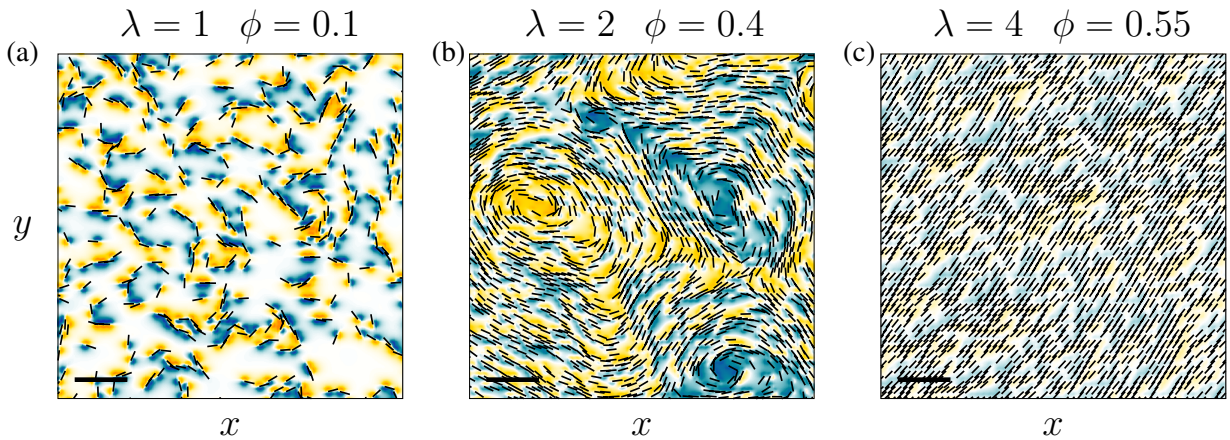

Figure 3: **Visualization of the mucus flow and ciliary-beat patterns** emerging in a periodic square computational domain. Three regimes are identified: (a) a poorly organized regime for $\lambda = 1$ and $\phi = 0.1$, (b) a swirly regime for $\lambda = 2$ and $\phi = 0.4$, and (c) a fully aligned regime for $\lambda = 4$ and $\phi = 0.55$. In each case, the flow is visualized by iso-contours of the non-dimensional vorticity ($\omega = [-0.5, 0.5]$), and black rods indicate beating directions. Part of the computational domain is shown and the scale bars correspond to $15D$.

4, ciliary beat directions tend to fully align over the whole domain. In this case, the flow is unidirectional and almost uniform. As a result, the flow is hardly sheared, as indicated by the low magnitude of the vorticity. The fully aligned regime is the only regime allowing an overall fluid transport. In this case, the average flow velocity can be computed analytically from the momentum balance, expressed as

$$\int_{\Omega_c} \boldsymbol{f_c} dS = \int_{\Omega} -\kappa \boldsymbol{U} dS, \tag{5}$$

where Ω and Ω_c are the total and ciliated surfaces. Assuming that the orientation of $\boldsymbol{f_c}$ is uniform over the domain, and aligned with the flow velocity $\boldsymbol{U}$, the average value of the velocity is

$$|\overline{\boldsymbol{U}}| = \frac{|\boldsymbol{f_c}|}{\kappa}\phi, \tag{6}$$

where the symbol $\overline{}$, in this equation and in the following, denotes the space-averaging operator. The mucus velocity is thus expected to linearly increase as a function of the ciliary density. In contrast, the mucus velocity appears to be independent of the mucus viscosity. This is an expected feature of the present model, which involves periodic boundary conditions, thus avoiding any energy dissipation due to boundary layers. Such dissipation is however expected to occur in real systems involving solid boundaries.

In order to quantitatively characterize the three regimes, two physical quantities are defined. The first one is the polarization $\mathcal{P}$,

$$\mathcal{P} = \left| \overline{\left(\frac{\boldsymbol{U}}{|\boldsymbol{U}|} \right)} \right|, \tag{7}$$

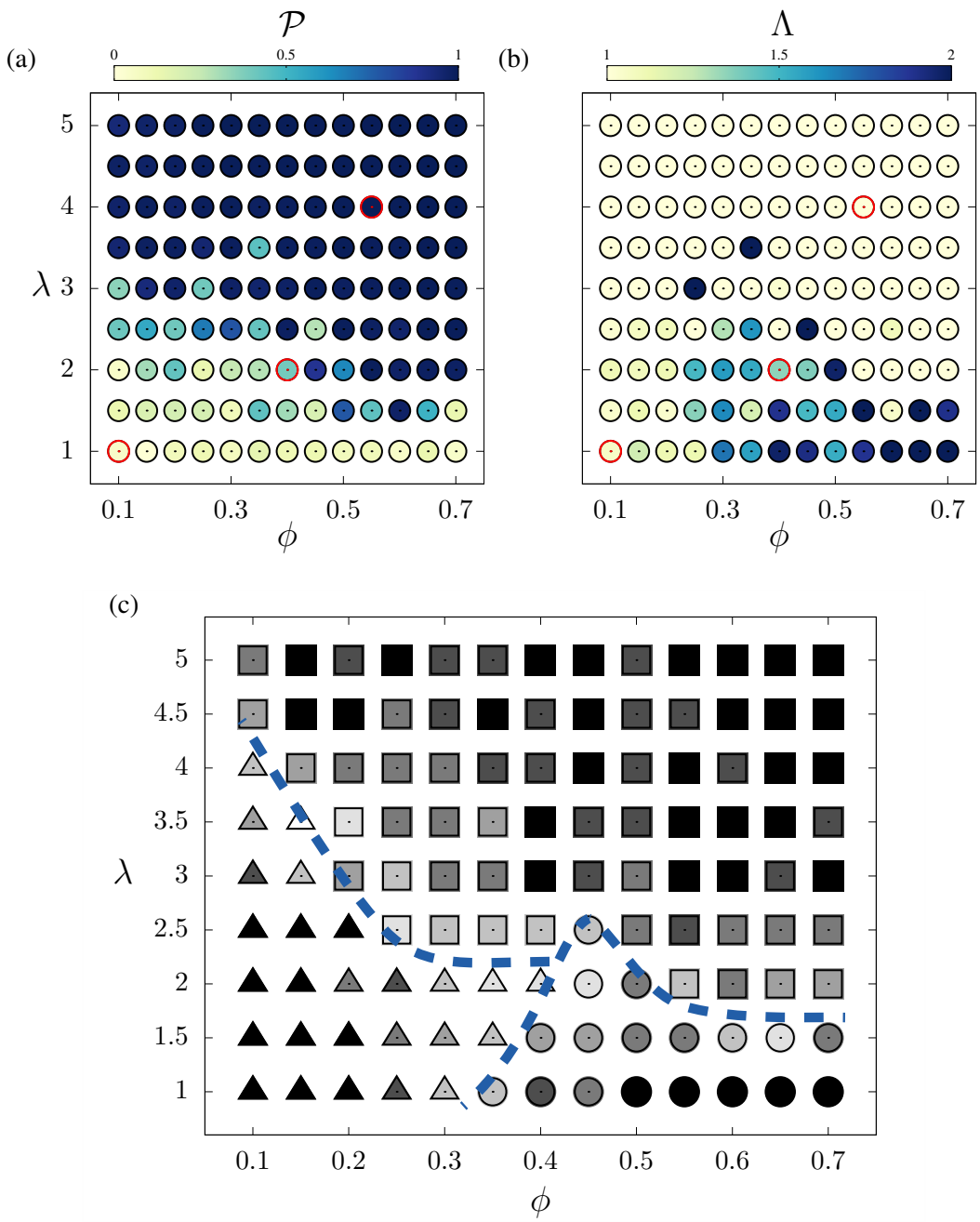

Figure 4: **Mapping of the regimes in the (ϕ, λ) parameter space**. Evolution of the (a) polarization $\mathcal{P}$ and (b) integral length Λ. The cases plotted in Fig. 3 are indicated by red circles. (c) Overview of the identified regimes based on Eq. 10; at each point, the most frequent regime over a set of ten randomly initialized runs is indicated by a triangle (poorly aligned), a circle (swirly) or a square (fully aligned) symbol. Symbols are colored using the occurrence frequency, ranging from 1/3 (white) to 1 (black). Dashed lines delimitate the three identified regions.

which is a spatial averaging of the unitary velocity vectors and quantifies the orientational order of the

overall flow. $\mathcal{P} \sim 1$ is a signature of a unidirectional flow. The second quantity, Λ, is defined as,

$$\Lambda = \sqrt{\frac{\kappa}{\mu_m}} \int_0^\infty \frac{R_x(\tau) + R_y(\tau)}{2} d\tau, \tag{8}$$

where $R_x(\tau)$ and $R_y(\tau)$ are auto-correlation functions of the vorticity along the x and y directions respectively.

$$R_x(\tau) = \frac{\overline{\omega(x,y)\omega(x+\tau,y)}}{\overline{\omega^2}}, \tag{9a}$$

$$R_y(\tau) = \frac{\overline{\omega(x,y)\omega(x,y+\tau)}}{\overline{\omega^2}}. \tag{9b}$$

Λ characterizes the typical length of large-scale flow structures and is a non dimensional integral length. In Eq. (8), it is normalized by $\sqrt{\mu_m/\kappa}$, the dimensional interaction length. Therefore, $\Lambda = 1$ indicates that the flow length scale corresponds to the range of influence of one ciliated element, i.e. no long-range dynamics occurs. In contrast, $\Lambda > 1$ indicates that large-scale vorticity regions are present, as in Fig. 3(b).

The evolutions of $\mathcal{P}$ and Λ in the (ϕ, λ) plane are plotted in Figs. 4(a) and 4(b), for λ ranging from 1 to 5, i.e. the range where regime transitions occur. From these variations, we identify three regions in the (ϕ, λ) space : the low-λ / low-ϕ region corresponds to a poorly organized regime, the low-λ / high-ϕ region corresponds to a swirly regime, and the high-λ / high-ϕ region corresponds to a fully aligned regime. We establish the flow regime phase diagram (Fig. 4(c)) by combining the two parameter $\mathcal{P}$ and Λ as following:

$$\begin{aligned} \mathcal{P} < 0.9, \;\; \Lambda < 1.5 &\Longleftrightarrow Poorly\ aligned, \\ \mathcal{P} < 0.9, \;\; \Lambda \geq 1.5 &\Longleftrightarrow Swirly, \\ \mathcal{P} \geq 0.9 &\Longleftrightarrow Fully\ aligned. \end{aligned} \tag{10}$$

Each point of the phase diagram represents the flow regime with the higher occurrence frequency among a series of ten randomly initialized runs. The greyscale used in Fig. 4(c) illustrates the sensitivity of the steady flow regime to initial conditions. As expected the flow regime is sensitive to the initial conditions close to the transition lines.

Ciliary beats align with the axis of a virtual airway

To get deeper insights in the role of the domain geometry on the flow direction in the fully aligned regime, we performed a series of 96 randomly initialized computations in a rectangular box with different aspect ratios. The aspect ratio is varied by increasing the domain size in the x direction (L_x); the domain size in the y direction (L_y) is kept constant. We use a box of the order of 2500 unit elements, with $\lambda = 5$ and $\phi = 0.4$ for which long-range fully aligned flow regime is predicted. For a square domain, no preferential flow direction is observed from one computation to the next one (Fig. 5(a)). When the aspect ratio of the domain is equal to 2 (Fig. 5(b)), a preferred flow direction emerges along the longest side of the domain.

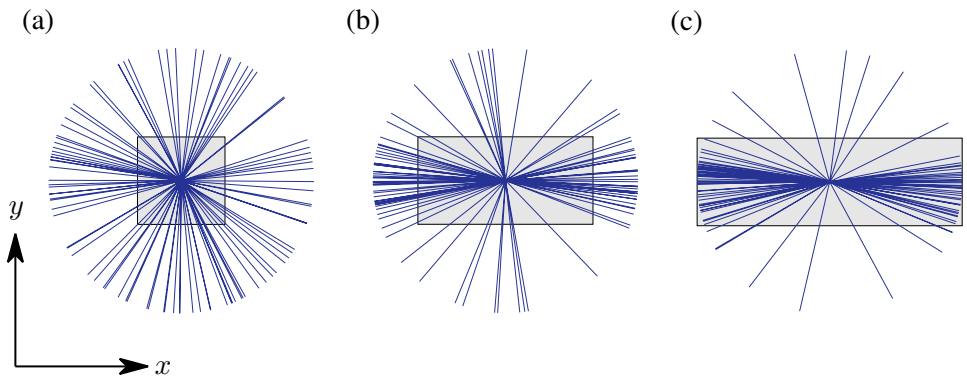

Figure 5: **Anisotropic confinement effect on the fully aligned solutions** in a $L_x \times L_y$ rectangular periodic domain, for $\lambda = 5$ and $\phi = 0.4$: (a) $L_x = L_y$, (b) $L_x = 2L_y$ and (c) $L_x = 3L_y$. In each case, the space-averaged flow directions issued from a series of 96 randomly initialized computations are represented by blue lines, and a gray rectangle indicates the geometry of the computational domain.

Upon further increase of the aspect ratio $L_x = 3L_y$ (Fig. 5(c)) the effect is even stronger and only 15 % of the independent calculations deviate from the preferential direction.

This alignment mechanism relates to an anisotropic confinement effect. Here, the term *confinement* is employed as the size of the periodic domain ($L_y/D = 50$) has an order of magnitude comparable to the range of influence of a ciliated element, determined by λ. Therefore, the periodicity of the domain has an influence on the ciliary organization. When the periodicity is anisotropic, the isotropy of the solution is lost, and a preferential direction spontaneously emerges.

The rectangular geometry is particularly interesting as it is a Cartesian representation of the surface of a circular tube aligned with the x axis. The y periodicity of the rectangle relates to the azimuthal periodicity of the tube, and thus depends on its diameter. In the x direction, the periodic boundary condition ensures that the flow is not constrained in this direction. The possible connections with a natural airway are further discussed hereafter.

Discussion

We proposed a hydrodynamic model to investigate the emergence of orientational order on a bronchial epithelium. It is based on the description of the two-dimensional mucus flow over an array of self-oriented momentum sources. The orientation of these driving forces is controlled by a streamwise-alignment rule, providing a hydrodynamic coupling between the flow and the ciliary forcing. The model is governed by two independent parameters, the ciliary density and the interaction length, related to the friction over the epithelium and depending on the mucus/PCL viscosity ratio.

The first main result of the model is that it predicts the three main flow regimes experimentally observed: (i) the local flow regime (Fig. 1(c)), (ii) the aligned flow (Figs. 1(a,b)), and (iii) the swirly regime observed at mesoscopic scale (Khelloufi et al., 2018).

This model predicts a fully aligned flow in mature epithelium ($\phi \in [0.5, 0.7]$) if λ is larger or equal to 2.

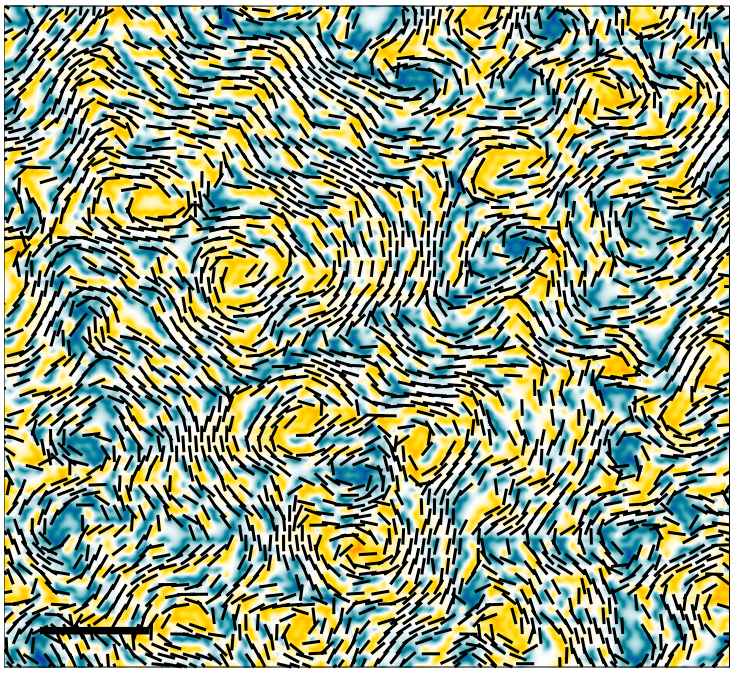

Figure 6: Visualization of the mucus flow and ciliary-beat pattern for $\phi = 0.7$ and $\lambda = 0.5$. This configuration is employed as a model of a the system after mucus removal (see Fig. 1(c)), i.e. when $\mu_m = \mu_p$. The flow is visualized using iso-contours of the non-dimensional vorticity ($\omega = [-2, 2]$), and black rods indicate beating directions. Part of the computational domain is shown and the scale bar corresponds to $15D$.

Physiologically, this minimal value of λ is expected to be reached in human airways since, as reported in the literature and discussed above, the values of $D \approx 2 \times 10^{-5}$m, $\delta_p \approx 10^{-5}$m, $\mu_p \sim 10^{-3}$Pa.s, and the mean $\mu_m \approx 1$Pa.s indeed lead to a mean $\lambda \approx 15$. When the mucus is removed, as in Fig. 1(c), the system can be modelled using $\mu_m = \mu_p$, leading to $\lambda \approx 0.5$. Even at high ciliary densities, only small mucus recirculations are predicted by the model in these conditions (see Fig. 6), which is consistent with the experimental observations.

Interestingly, the model predicts that the mucus viscosity tends to improve the directional organization of the epithelium, through an increase of the interaction length λ, thus enhancing the mucus clearance. On the other hand, mucus viscosity is often expected to have a detrimental effect on the clearance, mainly due to viscous dissipation in highly-sheared regions (boundary layers), that tends to decrease the transport velocity. These antagonistic mechanisms emphasize the possibly complex role of the viscosity in the mucus clearance process.

The role of the cilia density on long range mucus flow is also quantitatively described by the model. It could therefore be of interest for diseases affecting the motile cilia, for instance primary dyskenesia. Such a model can open the way to the prediction of the minimal density and spatial distribution of active cilia required to ensure a long-range mucus transport, i.e. the number of ciliated cells that has to be repaired on the airway.

A remarkable result of the model concerns the flow along rectangular domains with periodic boundary conditions. As stated above, this geometry can represent the 2D-developed geometry of a circular tube, similar to a natural airway. This comparison with a virtual human bronchus can be further analyzed by considering typical geometrical quantities. Indeed, an effect of the azimuthal periodicity on the directional organization is only expected if the periodicity length and the interaction length have comparable orders of magnitude. Based on the morphometric model of Weibel et al. (1963), the typical cross-section perimeter of human airways is expected to range from $L \approx 10^{-4}$m to $L \approx 10^{-2}$m (Karamaoun et al., 2016). By using $D \approx 2 \times 10^{-5}$m, the non-dimensional periodicity length is therefore expected to range from $L/D \approx 5$ to $L/D \approx 500$. This range is of the same order of magnitude as the expected range of interaction lengths in natural airway, namely $\lambda \in [1.5, 150]$ as discussed above. The results of the model therefore suggest that, in addition to the biologically driven phenomena occurring during airway development, the distal-proximal alignment of ciliary beats is favored by hydrodynamic interactions in a tube geometry.

Finally this work provides a model to predict the emergence of collective patterns for a class of original active matter systems which are characterized by non motile constitutive elements, yet exhibiting active dynamics. It predicts the spontaneous emergence of collective patterns and, strikingly, milling. It expands the class of the Vicsek-like models based on simple rules leading to milling and previously described by Costanzo and Hemelrijk (2018). This approach paves the way to the description of novel complex active systems made of non-motile active constituents where the interactions arise from a field of distant forces such as hydrodynamics or electromagnetics.

Materials and methods

Experimental methods

In-vitro bronchial epithelium

Mature commercial cultures (MucilAir) of reconstituted human bronchial epithelium from primary cells, were bought from Epithelix (Switzerland). The tissue is cultured at the Air Liquid Interface in a transwell of 6 mm in diameter. The apical side of the tissue is at the air interface and the basal side is in contact with the culture medium (Epithelix MucilAir culture medium) via a porous membrane. The culture medium (700 l) is replaced every two or three days. For experiments in absence of mucus, we removed the mucus by performing an apical washing. We added 200 l of culture medium on the apical side for 10 minutes, followed by three rinses with the culture medium. After an apical washing, a thin layer of medium culture ($\sim 10 - 40$ m) remains on top of the cilia. Experiments were repeated on three different cultures.

Imaging

We imaged the cultures in bright field on an inverted Nikon Eclipse Ti microscope with a x20 objective and a Luminera infinity camera. The temperature is maintained at 37 C and a humidified air flow of 5% CO2 is applied to maintain a physiological pH. To image the culture at the same place on different days, we used a motorized stage calibrated in the xy plane and saved the different positions.

Image processing

Beating directions of cilia were quantified using an in-house image processing routine applied on videomicroscopy acquisitions (40 fps). We first performed a standard deviation projection over 40 frames to reveal the trajectory of the tip of the cilia. Then we implemented in python the algorithm described in Püspöki et al. (2016) based on the structure tensor computation.

Numerical method

Lattice-Boltzmann method

The mucus flow, governed by Eq. (1), is simulated using a lattice-Boltzmann method (Krüger et al., 2017). This method, instead of directly describing the macroscopic flow behavior, is based on a mesoscopic description, namely a statistical description of the microscopic fluid particle dynamics. The particle distribution function $f(\boldsymbol{x}, \boldsymbol{\xi}, t)$ represents the density of fluid particles with velocity $\boldsymbol{\xi}$ at location $\boldsymbol{x}$ and time t. Its dynamics is governed by the Boltzmann equation, which in the absence of external forcing writes

$$\frac{\partial f}{\partial t} + \boldsymbol{\xi} \cdot \boldsymbol{\nabla} \boldsymbol{f} = \Gamma(f), \tag{11}$$

where Γ designates the collision operator. At the macroscopic level, the Boltzmann equation is equivalent to the Navier-Stokes equations, and it is thus relevant to describe the present mucus flow.

The discretization of (11) in velocity space, physical space and time leads to the lattice-Boltzmann equation. The velocity space is discretized on a set of velocity vectors $\{\boldsymbol{c_l}, l = 0, ..., Q-1\}$, where Q is the number of discrete velocities. In the present work, a $D2Q9$ velocity set is used, in which the velocity space is discretized by nine velocities, namely

$$\boldsymbol{c_l} = \begin{cases} (0,0), & l = 0, \\ c\left(\cos(\frac{\pi(l-1)}{2}), \sin(\frac{\pi(l-1)}{2})\right), & l \in [1,4], \\ \sqrt{2}c\left(\cos(\frac{\pi(2l-9)}{4}), \sin(\frac{\pi(2l-9)}{4})\right), & l \in [5,8], \end{cases} \tag{12}$$

where c is the lattice speed, and $\boldsymbol{e_x}$ and $\boldsymbol{e_y}$ are unit vectors in the x and y directions. The particle densities at velocities $\{\boldsymbol{c_l}\}$ are represented by the discrete-velocity distribution functions $\{f_l(\boldsymbol{x}, t)\}$, also called particle populations. Time and space are discretized so that particle populations are transported from one node to a neighboring one during one time step, namely $\Delta x/\Delta t = \Delta y/\Delta t = c$. The associated grid is thus Cartesian and uniform. The grid spacing is denoted by $\Delta n = \Delta x = \Delta y$. In the following, all quantities are normalized by c and Δt, so that $\Delta n = \Delta t = 1$.

Using this normalization, the lattice-Boltzmann equation writes

$$f_l(\boldsymbol{x} + \boldsymbol{c_l}, t+1) - f_l(\boldsymbol{x}, t) = \Gamma_l(\boldsymbol{x}, t) \tag{13}$$

where Γ_l is the discretized collision operator. The left-hand side of (13) describes the streaming step; the right-hand side is the collision step. Equation (13) is explicit, and the streaming and collision steps can be treated separately.

The macroscopic flow quantities are moments of the particle populations in the velocity space. In particular, the fluid momentum $\rho_m \boldsymbol{U}$ and density write

$$\rho_m \boldsymbol{U} = \sum_{l=0}^{8} f_l \boldsymbol{c_l}, \quad \rho_m = \sum_{l=0}^{8} f_l. \tag{14}$$

Even though the lattice-Boltzmann method allows small variations of the fluid density, in practice these variations are negligible if the flow velocity remains small, and the fluid can be considered as close to incompressible.

In the present simulations, a Bhatnagar-Gross-Krook (BGK) collision operator is employed, namely

$$\Gamma_l(\boldsymbol{x}, t) = \frac{1}{\tau}\left(f_l(\boldsymbol{x}, t) - f_l^{(eq)}(\boldsymbol{x}, t)\right), \tag{15}$$

where τ is called the relaxation time and determines the kinematic fluid viscosity through $\nu_m = \frac{1}{3}(\tau - 1/2)$, using the present normalization, and $f^{(eq)}$ denotes the equilibrium particle distribution function, expressed as

$$f_l^{(eq)} = w_l \rho_m \left(1 + \frac{\boldsymbol{U} \cdot \boldsymbol{c_l}}{c_s^2} + \frac{(\boldsymbol{U} \cdot \boldsymbol{c_l})^2}{2c_s^4} - \frac{\boldsymbol{U} \cdot \boldsymbol{U}}{2c_s^2}\right). \tag{16}$$

The weights $\{w_l\}$ are specific to the velocity set. In the present case ($D2Q9$ velocity set), $w_0 = 4/9$, $w_1 = w_2 = w_3 = w_4 = 1/9$ and $w_5 = w_6 = w_7 = w_8 = 1/36$.

Inclusion of an external forcing

The effect of the body force $\boldsymbol{f_n}$ is ensured by the external forcing scheme proposed by Guo et al. (2002). The lattice-Boltzmann equation becomes

$$f_l(\boldsymbol{x}+\boldsymbol{c_l},t+1)-f_l(\boldsymbol{x},t)=\Gamma_l(\boldsymbol{x},t)+\left(1-\frac{1}{2\tau}\right)S_l(\boldsymbol{x},t), \tag{17}$$

where S_l is a source term expressed as

$$S_l=w_l\left(\frac{\boldsymbol{c_l}-\boldsymbol{U}}{c_s^2}+\frac{(\boldsymbol{c_l}\cdot\boldsymbol{U})\cdot\boldsymbol{c_l}}{c_s^4}\right)\cdot\boldsymbol{f_n}. \tag{18}$$

The flow momentum has to be corrected according to the external forcing, following

$$\rho_m\boldsymbol{U}=\sum_{l=0}^{8}f_l\boldsymbol{c_l}+\frac{1}{2}\boldsymbol{f_n}. \tag{19}$$

As described in *Hydrodynamic model of ciliary-beat organization*, the forcing $\boldsymbol{f_n}$ is decomposed in two parts, i.e. the ciliary force $\boldsymbol{f_c}$ and the friction force $\boldsymbol{f_v}$. However, the friction depends on the fluid velocity, namely $\boldsymbol{f_v}=-\kappa\boldsymbol{U}$. Therefore, the flow momentum can be expressed as

$$\rho_m\boldsymbol{U}=\frac{\sum_{l=0}^{8}f_l\boldsymbol{c_l}+\frac{1}{2}\boldsymbol{f_c}}{1+\kappa/2\rho_m}. \tag{20}$$

Algorithm and numerical parameters

A summary of the implemented algorithm is proposed in table 1. During the initialization, the ciliated elements are randomly placed in the computational domain. An example of initialization is shown in Fig. 7(a). A closer view of the hexagonal mesh and underlying fluid nodes is given in Fig. 7(b). The distance between two neighboring nodes, in the x or y direction, is denoted by Δn; it is set to $\Delta n=D/5$, where D denotes the side length of the hexagonal elements. At each time step, the flow velocity is averaged in each ciliated elements, and the angle of the ciliary forcing is updated following Eq. (2). The parameter Ω, which drives the transient re-orientation of the ciliated elements but does not affect the final steady solution, is set to $\Omega=U_0/D$. It is recalled that U_0 designates the typical mucus velocity. A small threshold angle is employed, namely $\theta_0=2\Omega\Delta t=0.004$ radians using the present numerical parameters, so that its influence on model solutions can be neglected. The number of performed time steps varies from one computation to the other, since simulations are systematically continued until a steady solution is reached. This is achieved by checking the statistical convergence of several global quantities as the total fluid kinetic energy, the total flow rate and the space-average instantaneous variation of the ciliary-force orientations.

Supplemental material

Video 1 – Transport of mucus above beating cilia corresponding to the field of view of the figure 1(a) & 1(b). The movie is accelerated 150 times. The still image on the right panel corresponds to the projection

1. At the beginning of the computation, the fluid velocity is set to zero, and the particle populations are equal to the equilibrium distributions (16).

2. The hexagonal mesh is initialized, and the ciliated elements are randomly selected according to the prescribed ciliary density. The ciliary forces are initialized with random orientations. The ciliary forces are transferred from the hexagonal mesh to the fluid nodes.

3. The time-marching loop is performed until the prescribed number of time steps is achieved :

3.1. The ciliary forces are updated according to Eq. (2):

3.1.1. On each ciliated cell i, the space-averaged flow velocity is computed to determine the local flow orientation angle θ_f^i.

3.1.2. The misalignment $\Delta\theta^i$ is computed, and the new ciliary force orientation is determined accordingly.

3.1.3. The updated ciliary forces are transferred from the hexagonal mesh to the fluid nodes.

3.2. Collision is performed (15)

3.3. Streaming is performed (13).

3.4. Macroscopic quantities are computed (14,19), and the friction force $\boldsymbol{f_v}$ is updated.

4. Output of the final solution (flow velocity, ciliary forces, etc).

Table 1: Summary of the present numerical algorithm.

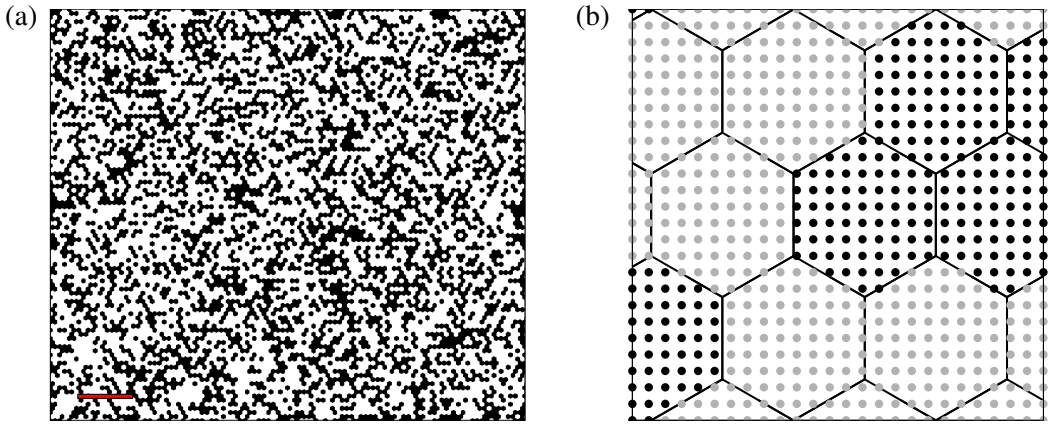

Figure 7: **Spatial discretization employed in the model** (a) Visualization of the numerical domain, for a ciliary density $\phi = 0.4$. The epithelium is discretized using hexagonal elements, representing cells or groups of cells. The ciliated elements, indicated in black, are randomly placed during the initialization of the computations. The scale bar corresponds to $20D$. (b) Closer visualization representing the hexagonal elements and the underlying numerical grid. On ciliated elements, the ciliary forcing is locally imposed on lattice nodes, indicated by black points. On non-ciliated elements (grey points), the ciliary forcing vanishes. The side length of hexagonal elements is equal to D.

of 20 frames of the movie of mucus transport using a standard deviation projection method to determine the streamlines of the mucus. The scale bars are 20 m.

Video 2 – Beating cilia on in-vitro reconstituted human bronchial epithelium cultures. Left, center and right panels corresponds to the field of views of the figure 1a, 1b and 1c respectively. The total time of the movie is 2.5s and scale bars are 20 m.

Video 3 – Time-evolution of the mucus flow and ciliary-forcing directions, for $\phi = 0.5$ and $\lambda = 1$. The flow is visualized using iso-contours of the flow velocity magnitude, and black rods indicate beating directions.

Video 4 – Time-evolution of the mucus flow and ciliary-forcing directions, for $\phi = 0.5$ and $\lambda = 2$. The flow is visualized using iso-contours of the flow velocity magnitude, and black rods indicate beating directions.

Video 5 – Time-evolution of the mucus flow and ciliary-forcing directions, for $\phi = 0.5$ and $\lambda = 4$. The flow is visualized using iso-contours of the flow velocity magnitude, and black rods indicate beating directions.

Acknowledgments

The project MACBION leading to this publication has received funding from Excellence Initiative of Aix-Marseille University - A*MIDEX, a French Investissements d'Avenir programme, the LABEX

MEC, and the SINUMER project (ANR-18-CE45-0009-01) of the French National Research Agency (ANR).

References

Adam Wanner, Matthias Salathé, and Thomas G O'Riordan. Mucociliary clearance in the airways. *American Journal of Respiratory and Critical Care Medicine*, 154(6):1868–1902, 1996.

P Chanez. Severe asthma is an epithelial disease. *European Respiratory Journal*, 25:945–946, 2005.

James C Hogg, Fanny Chu, Soraya Utokaparch, Ryan Woods, W Mark Elliott, Liliana Buzatu, Ruben M Cherniack, Robert M Rogers, Frank C Sciurba, Harvey O Coxson, et al. The nature of small-airway obstruction in chronic obstructive pulmonary disease. *New England Journal of Medicine*, 350(26): 2645–2653, 2004.

JA Regnis, M Robinson, DL Bailey, P Cook, P Hooper, HK Chan, I Gonda, G Bautovich, and PT Bye. Mucociliary clearance in patients with cystic fibrosis and in normal subjects. *American Journal of Respiratory and Critical Care Medicine*, 150(1):66–71, 1994.

Richard C Boucher. Airway surface dehydration in cystic fibrosis: pathogenesis and therapy. *Annual Review of Medicine*, 58:157–170, 2007.

Hirotoshi Matsui, Scott H Randell, Steven W Peretti, C William Davis, and Richard C Boucher. Coordinated clearance of periciliary liquid and mucus from airway surfaces. *The Journal of Clinical Investigation*, 102(6):1125–1131, 1998.

Mustapha-Kamel Khelloufi, Etienne Loiseau, Marc Jaeger, Nicolas Molinari, Pascal Chanez, Delphine Gras, and Annie Viallat. Spatiotemporal organization of cilia drives multiscale mucus swirls in model human bronchial epithelium. *Scientific Reports*, 8(1):2447, 2018.

John B Wallingford. Planar cell polarity signaling, cilia and polarized ciliary beating. *Current Opinion in Cell Biology*, 22(5):597–604, 2010.

Nathalie Spassky and Alice Meunier. The development and functions of multiciliated epithelia. *Nature Reviews Molecular Cell biology*, 18(7):423, 2017.

Regina Faubel, Christian Westendorf, Eberhard Bodenschatz, and Gregor Eichele. Cilia-based flow network in the brain ventricles. *Science*, 353(6295):176–178, 2016.

Boris Guirao, Alice Meunier, Stéphane Mortaud, Andrea Aguilar, Jean-Marc Corsi, Laetitia Strehl, Yuki Hirota, Angélique Desoeuvre, Camille Boutin, Young-Goo Han, et al. Coupling between hydrodynamic forces and planar cell polarity orients mammalian motile cilia. *Nature Cell Biology*, 12(4):341, 2010.

Brian Mitchell, Richard Jacobs, Julie Li, Shu Chien, and Chris Kintner. A positive feedback mechanism governs the polarity and motion of motile cilia. *Nature*, 447(7140):97, 2007.

Tamás Vicsek and Anna Zafeiris. Collective motion. *Physics Reports*, 517(3-4):71–140, 2012.

David JT Sumpter. *Collective animal behavior*. Princeton University Press, 2010.

David Saintillan. Rheology of active fluids. *Annual Review of Fluid Mechanics*, 50:563–592, 2018.

Tamás Vicsek, András Czirók, Eshel Ben-Jacob, Inon Cohen, and Ofer Shochet. Novel type of phase transition in a system of self-driven particles. *Physical Review Letters*, 75(6):1226, 1995.

A Costanzo and CK Hemelrijk. Spontaneous emergence of milling (vortex state) in a vicsek-like model. *Journal of Physics D: Applied Physics*, 51(13):134004, 2018.

Yang Ding, Janna C Nawroth, Margaret J McFall-Ngai, and Eva Kanso. Mixing and transport by ciliary carpets: a numerical study. *Journal of Fluid Mechanics*, 743:124–140, 2014.

Sylvain Chateau, Julien Favier, Umberto D'Ortona, and Sébastien Poncet. Transport efficiency of metachronal waves in 3d cilium arrays immersed in a two-phase flow. *Journal of Fluid Mechanics*, 824:931–961, 2017.

Boris Guirao and Jean-François Joanny. Spontaneous creation of macroscopic flow and metachronal waves in an array of cilia. *Biophysical journal*, 92(6):1900–1917, 2007.

Tina Raman, Timothy P O'Connor, Neil R Hackett, Wei Wang, Ben-Gary Harvey, Marc A Attiyeh, David T Dang, Matthew Teater, and Ronald G Crystal. Quality control in microarray assessment of gene expression in human airway epithelium. *BMC genomics*, 10(1):493, 2009.

Michelle R Staudt, Allison Rogalski, Ann E Tilley, Robert J Kaner, Ben-Gary Harvey, and Ronald G Crystal. C26 tobacco: How it harms us and more reasons to quit: Smoking is associated with a loss of ciliated cells throughout the airways. *American Journal of Respiratory and Critical Care Medicine*, 189:1, 2014.

Brian Button, Li-Heng Cai, Camille Ehre, Mehmet Kesimer, David B Hill, John K Sheehan, Richard C Boucher, and Michael Rubinstein. A periciliary brush promotes the lung health by separating the mucus layer from airway epithelia. *Science*, 337(6097):937–941, 2012.

Samuel K Lai, Ying-Ying Wang, Denis Wirtz, and Justin Hanes. Micro-and macrorheology of mucus. *Advanced Drug Delivery Reviews*, 61(2):86–100, 2009.

Ewald R Weibel, André Frédérick Cournand, and Dickinson W Richards. *Morphometry of the human lung*, volume 1. Springer, 1963.

Cyril Karamaoun, Alain Van Muylem, and Benoît Haut. Modeling of the nitric oxide transport in the human lungs. *Frontiers in Physiology*, 7:255, 2016.

Zsuzsanna Püspöki, Martin Storath, Daniel Sage, and Michael Unser. Transforms and operators for directional bioimage analysis: a survey. In *Focus on Bio-Image Informatics*, pages 69–93. Springer, 2016.

Timm Krüger, Halim Kusumaatmaja, Alexandr Kuzmin, Orest Shardt, Goncalo Silva, and Erlend Magnus Viggen. *The Lattice Boltzmann Method: principles and practice*. Springer, 2017.

Zhaoli Guo, Chuguang Zheng, and Baochang Shi. Discrete lattice effects on the forcing term in the lattice boltzmann method. *Physical Review E*, 65(4):046308, 2002.